and J. B. Pendry, Solid State Commun. **9**, 1851 (1971).

[24]In the case where two different subplanes lie in the same x-y plane, i.e., $\vec{d}_\alpha^\perp = \vec{d}_{\alpha'}^\perp$, the matrix $G_{LL'}^{\alpha\alpha'}(\vec{k}_j)$ should be evaluated in real space using an expression similar to that given in Eq. (13). But in this paper, we shall assume that different subplanes have different $d_\alpha^{||}$. We shall also assume that $\vec{d}_\alpha = a(\vec{d}_P + d_z \vec{e}_\perp)$, where d_z and $\vec{d}_P$ are the Z-spacing and the two-dimensional shift of the origin between successive subplanes, respectively.

[25]For most materials, the electron mean free path is about

4-6 Å in the energy range 20-200 eV; see, for example, P. W. Palmberg and T. N. Rhodin, J. Appl. Phys. **39**, 2425 (1967).

[26]E. T. Whittaker and G. N. Watson, *A Course of Modern Analysis* (Cambridge U. P., London, 1927), p. 326.

[27]See, for example, A. Messiah, *Quantum Mechanics* (Wiley, New York, 1961), p. 495.

[28]G. N. Watson, *Theory of Bessel Functions*, 2nd ed. (Cambridge U. P., London, 1944).

[29]J. L Beeby, Proc. R. Soc. A **279**, 82 (1964).

Application of the t-Matrix Perturbation Method to the Analysis of Low-Energy-Electron-Diffraction Spectra for Aluminum*

S. Y. Tong[†] and T. N. Rhodin

School of Applied and Engineering Physics, Cornell University, Ithaca, New York 14850

R. H. Tait[‡]

Department of Physics, Cornell University, Ithaca, New York 14850

(Received 24 October 1972)

The t-matrix perturbation method developed in the preceding paper is applied to the calculation of low-energy-electron-diffraction spectra for different beams on different faces of aluminum for a wide range of angles of incidence. The dynamical model used in the theoretical method is illustrated in detail and effects of dynamical factors are analyzed. Comparisons between theory and experiment of the spectra indicate good agreement for all beams for Al(001) for a wide range of incident angles. Reasonable agreement is obtained for the (110) face although some discrepancies are observed in peak positions and in peak profiles at low energies.

I. INTRODUCTION

A low-energy electron, typically in the energy range between a few eV to a few hundred eV above the vacuum level, incident on a crystal, penetrates only a few surface layers of the solid.[1] This small penetration distance is the consequence of strong electron-electron interaction between the incident electron and valence electrons of the solid. The mean free path of the incident electron is inversely proportional to the imaginary part of the optical potential of the solid.[2,3] In principle, such localization of the incident-electron wave field to the surface region makes low-energy-electron diffraction (LEED) a powerful means for the study of surface properties of target materials. However, since real surfaces are highly nonhomogeneous and irregular on an atomic scale, interactions in the surface region are predominantly nonlocal and require an approach leading to a many-body self-consistent solution. There have been encouraging improvements in recent years in the modeling of surfaces,[4,5] mainly in the use of one-body local Hamiltonians applied to the self-consistent solution of surface valence charge densities and surface potentials for free-electron metals. In comparison to such recent theoretical surface models, the usual surface model used in LEED calculations appears rather simple and almost crude. The usual surface model used in LEED theory consists of planes of bulk ion cores stacked in bulk spacings and terminated at a given surface plane. A uniform electron gas with charge density corresponding to that of a jellium model for the valence electrons of the material extends throughout the planes of ion cores. The uniform electron gas is terminated in terms of a step function at a given distance beyond the centers of surface ion cores. Beyond this surface plane, there is assumed to be a vacuum region extending to infinity. Such a surface model gives erroneous results for the surface potential and the charge density of valence electrons at the interface, since in real solids both the charge density and the surface potential vary smoothly and rapidly from their bulk values to their values in vacuum. Also, this simple surface model gives drastic results if applied to chemisorption since the lack of self-consistency in surface valence-electron wave functions and the oversimplified assumption of a uniform surface which neglects strong localized interactions, leads to unphysical predictions both in the binding energy and in the amount of charge transfer. However, a number of recent microscopic calculations[6] in LEED using such a model for the surface have been surprisingly successful, nevertheless, in obtaining good agreement between theory

and experiment for the intensity-energy spectra for clean surfaces of different materials. Why then would such a simple surface model do so well in low-energy-electron-diffraction calculations in view of the previous considerations? The answer relates to the fact that in low-energy-electron diffraction, we are primarily dealing with backscattering properties of the solid in the surface region. It is electrons in the ion cores that turn the incident electrons around, and the exact nature of the interface is not of primary importance. In most materials, electrons in ion cores are not that much perturbed by the presence of the surface. The valence electrons, on the other hand, contribute largely to forward scattering processes, which in turn contribute to LEED spectra through multiple scattering events. The use of a uniform-electron-gas model neglects the tail of the valence charge density at the interface region. Fortunately, the effect of this tail on the average charge density per unit cell is small. It is significant only for individual valence wave functions at the interface. For present purposes, it is therefore sufficient to note that this simple model for the surface seems to work well in terms of scattering properties of low-energy-electron diffraction from solids. This observation brings out the important concept that the apparent insensitivity of LEED spectra to local details of surface valence charge densities and their strong dependence on electron ion cores make low-energy-electron diffraction an effective way to study *locations* of surface atoms, both on clean surfaces and in adsorbed layers. Whereas a host of surface phenomena such as chemisorption,[7-12] resonance field emission,[13] photoemission,[14,15] ion-neutralization spectroscopy,[16,17] and inelastic LEED[18,19] reflect mainly electronic properties in the surface region, elastic low-energy-electron diffraction, on the other hand, is unique in its suitability for structural analysis of surface atoms. However, one must exercise a degree of caution in that certain dynamical factors can indeed have important effects in a LEED calculation.[20] Such factors and their effects on the determination of surface structure from LEED spectra are analyzed and discussed in Secs. II and III of this paper.

In the preceding paper,[31] we presented the theoretical formalism of a third-order perturbation method within the microscopic approach to LEED. In this paper, we shall apply this method to the calculation of LEED spectra for a simple metal. The organization of the body of this paper is as follows. In Sec. II, we describe and list the model of dynamical factors used in this calculation. In Sec. III, we analyze the effects of such dynamical factors on the accuracy with which theoretical values may be meaningfully compared with experimental results. In Sec. IV, we describe the computation

procedure of the *t*-matrix method, and in Sec. V, we present results of a detailed comparison of LEED intensity spectra between theory and experiment for a wide range of incident angles and for different reflected beams and different faces of aluminum. Finally, in Sec. VI, we summarize our findings and give a critique of our results.

II. DYNAMICAL MODEL IN LEED THEORY

In this section we list and describe the dynamical quantities in our model. While the discussion in this section is presented with reference to the specific dynamical model we chose for this calculation, the general physical concepts are, in most cases, applicable to all microscopic approaches in LEED.

A. Crystal Potential

In our model, the solid is divided into Wigner–Seitz cells containing nonoverlapping muffin-tin spheres. Scattering between the incident electron and each Wigner–Seitz unit cell of the solid is described in terms of energy-dependent phase shifts.[20] The phase shifts are obtained by integrating the radial part of Schrödinger's equation containing the single-site scattering potential in the muffin-tin approximation for each partial wave and at each energy. This means that multiple scattering events within each muffin-tin site are included to infinite order. For the single-site muffin-tin potential, we use a full Hartree–Fock potential constructed by Pendry[21] which does not use the local-exchange approximation. The use of such a potential is well documented in other materials.[22,23] In Fig. 1, we show the first six partial-wave phase shifts calculated from this potential for aluminum in the energy range 0–200 eV measured with respect to the muffin-tin zero of energy. In this energy range, the dominant partial wave is the $(l = 2)$ d wave.[20] We limit ourselves in this calculation to six partial waves mainly because in this given energy range, higher partial waves are small and have nonconsequential contributions to the intensity-energy spectra. Our method, on the other hand, is so fast that we can handle many additional partial waves, if necessary, with relative ease.

B. Model for the Surface

The main features of the surface model used in this calculation are described briefly in the Introduction. The bulk muffin-tin potential is assumed to extend unperturbed up to the surface plane. A uniform electron gas made up from the valence charge density of each ion core extends slightly beyond the plane of surface ion cores. In this calculation, we have put the cutoff plane of the uniform electron gas at a distance equal to the bulk interlayer spacing from the centers of the surface ion

cores.[20] Schematic illustrations of this surface model for the (001) and (110) faces of aluminum are shown in Fig. 2. Following this model, surface ion cores in the (110) face are just covered by the electron gas [Fig. 2(b)], while in the (001) face, the uniform electron gas extends a distance of 0.591 Å beyond the surface layer of muffin-tin spheres [Fig. 2(a)]. The incident electrons, when passing through the uniform electron gas, lose flux from the elastic beam owing to inelastic excitation processes. Thus, where one places the cutoff plane for the electron gas determines the over-all absolute reflectivity of the calculated spectra. In Sec. III, we shall discuss magnitudes for absolute reflectivities in terms of different positions of the electron cutoff plane.

C. Surface Barrier

In this calculation, we shall assume no back re-flection at the interface between vacuum and the uniform electron gas. Although the incident elec-tron does undergo a Snell's refraction at the inter-face owing to the presence of an inner potential,[24] we shall assume no back reflection at the interface. In other words, all physical scatterings are as-sumed to come from the muffin-tin potentials. Our assumption is based on the fact that in real sur-faces, the surface-barrier potential varies rather smoothly from its bulk value inside the solid to the vacuum level outside. This smooth variation of the barrier potential cuts down drastically, surface reflections at the interface.[25] Thus, the nonreflec-tion model is a rather good approximation of the true reflection conditions at real surfaces. This model has been applied with considerable success in the case of aluminum.[20,26-28] In a more realistic model for the surface barrier, one should not elim-
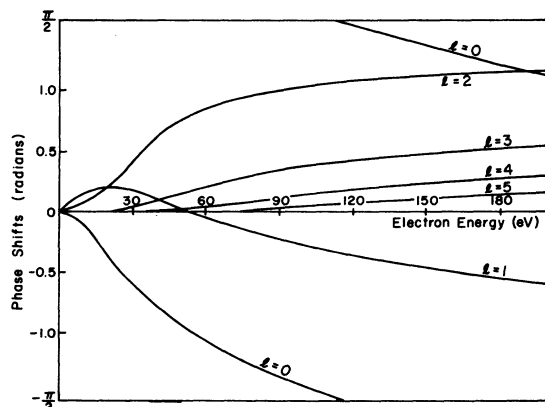

FIG. 1. First six phase shifts of aluminum expressed modulo π, plotted in the energy range 0–200 eV measured with respect to the muffin-tin zero. A Hartree–Fock po-tential, Ref. 21, is used to calculate the phase shifts.

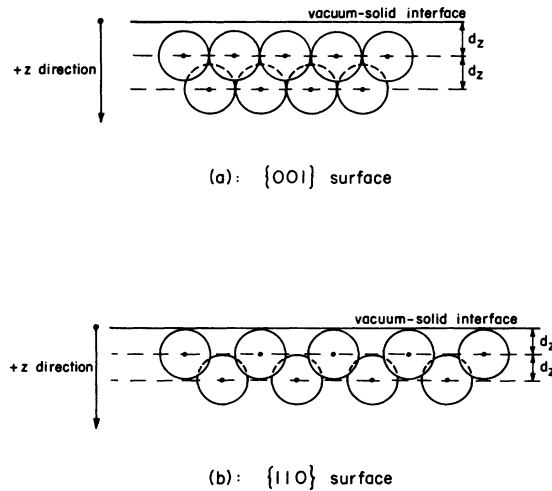(a): {OOI} surface

(b): {IIO} surface

FIG. 2. Surface model (a) for the Al(001) face and (b) for the Al(110) face. The positive Z direction is mea-sured inwards from the vacuum-solid interface.

inate all reflections at the barrier, but should in-stead calculate surface reflections from some smoothly varying shape of the surface-barrier po-tential.

D. Inelastic Electron Damping

Inside the solid, the incident electron interacts with the electron gas and excites a series of inelas-tic processes. These inelastic processes remove energy from the incident-electron beam and trans-fer electrons from the elastic flux into inelastically scattered electrons. The two most important in-elastic processes inside the solid are single-parti-cle excitations and bulk-plasmon emissions.[29,30] In the surface region and at large angles of inci-dence, surface-plasmon emissions are also be-lieved to be important. In our present treatment, we do not, however, include effects of surface plasmons. Inclusion of such a relatively unknown dynamical factor in our present model would nec-essarily introduce an adjustable parameter into our discussion.[20] In this calculation, damping ef-fects due to single-particle and bulk-plasmon exci-tations are included in terms of the imaginary part of an effective electron self-energy.[31] A complete calculation for the self-energy of a uniform electron gas was done numerically by Lundqvist[30] in the ran-dom-phase approximation for a set of metallic den-sities and for energies and momenta ranging from zero to a few hundred eV above the Fermi level. If we write the self-energy of a uniform electron gas as $M(\vec{k}, E) = M_1(\vec{k}, E) + i M_2(\vec{k}, E)$, then the effective self-energy $\Sigma(\vec{k}, E) = \Sigma_1(\vec{k}, E) + i \Sigma_2(\vec{k}, E)$ used in our model has the same imaginary part, i.e., $\Sigma_2(\vec{k}, E)$ $= M_2(\vec{k}, E)$. We define the real part of $\Sigma(\vec{k}, E)$ as the inner potential of our model. It is related to

the real part of $M(\vec{k}, E)$ by[32]

$$|\Sigma_1(\vec{k}, E)| = |M_1(\vec{k}, E)| + |D| - \delta, \tag{1}$$

where $|D|$ is the self-consistent solution of the dipole potential at the surface and $\delta = V_M - \Gamma$ is the difference between the muffin-tin average V_M of the crystal and the bottom of the conduction band Γ.

The self-energy $M(\vec{k}, E) = M(k, E)$ of a uniform electron gas satisfies the dispersion relation[30]

$$\hbar^2 k^2/2m = E - M(k, E - \epsilon_0). \tag{2}$$

For fixed k, one may expand $M(k, E)$ to first order in the difference $E - \epsilon_0 - \hbar^2 k^2/2m$ and obtain[30]

$$\hbar^2 k^2/2m = E - M^*(k, \hbar^2 k^2/2m), \tag{3}$$

where

$$M^*(k, \hbar^2 k^2/2m) = Z(k)M(k, \hbar^2 k^2/2m) + \epsilon_0[1 - Z(k)]. \tag{4}$$

In Eqs. (2) and (4), we have put

$$Z(k) = \left(1 - \frac{\partial M(k, E)}{\partial E}\Bigg|_{E = \hbar^2 k^2/2m}\right)^{-1}$$

and

$$\epsilon_0 = M(k_F, \hbar^2 k_F^2/2m),$$

where k_F is the Fermi momentum.[20] One should note that by the use of the complex quasiparticle renormalization factor $Z(k)$, the renormalized self-energy $M^*(k, \hbar^2 k^2/2m)$ depends only on momentum k. The dispersion relation given in Eq. (3) may be solved self-consistently for given values of E. Using Eqs. (1) and (4), we can define a $\Sigma^*(k, \hbar^2 k^2/2m)$ as

$$|\Sigma_1^*(k, \hbar^2 k^2/2m)| = |M_1^*(k, \hbar^2 k^2/2m)| + |D| - \delta \tag{5}$$

and

$$\Sigma_2^*(k, \hbar^2 k^2/2m) = M_2^*(k, \hbar^2 k^2/2m). \tag{6}$$

In Fig. 3, we show the values of $M(k, \hbar^2 k^2/2m)$ and $Z(k)$ as functions of k/k_F for an electron density corresponding to that of metallic aluminum. The variation in energy of $M(k, \hbar^2 k^2/2m)$ corresponds to the sum of the energy dependences of both exchange and correlation effects of the electron gas. In Fig. 3, we see that at near the Fermi level, $M_1(k, \hbar^2 k^2/2m)$ is almost constant with energy. This is due to near cancellations in the energy dependences of exchange and correlation energies at near "band-structure" energies, i.e., $E \approx E_F$.[33] However, we see from Fig. 3 that at $k \geq 1.7 k_F$, the sum of exchange and correlation energies begins to increase as a whole with energy. The sum is negative, so the absolute value of the sum actually decreases as the energy increases.

Our use of a momentum- and energy-dependent inner potential is different from that used in other calculations,[22,26,27] but is consistent with the objective of achieving a parameter-free model. From

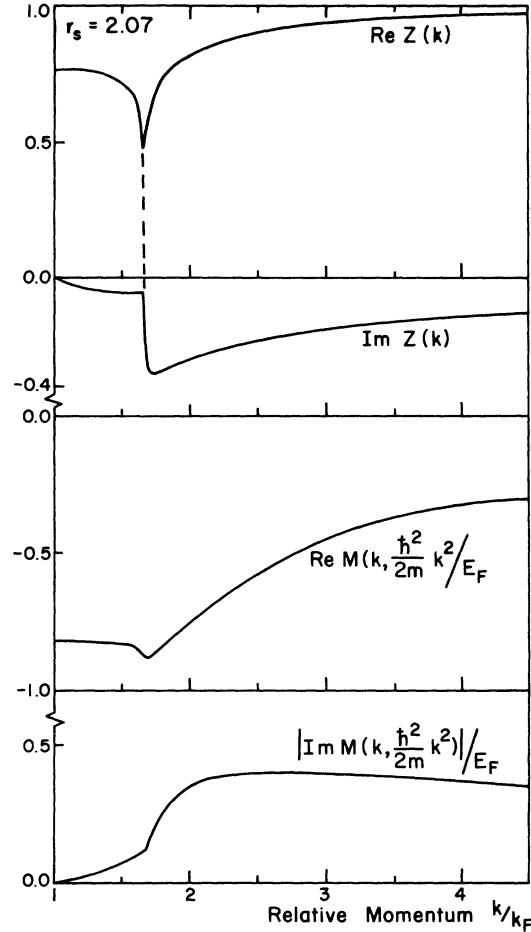FIG. 3. Electron self-energy $M(k, \hbar^2 k^2/2m)$ and complex quasiparticle renormalization factor $Z(k)$ plotted as a function of relative momentum k/k_F.

band-structure calculations,[34-37] it is known that metallic aluminum has free-electron-like valence electrons. One would then expect the electron-gas calculation for the self-energy[30] used here to have some validity. For example, from Eq. (4), we find that at the Fermi level, $|M_1^*(k_F, \hbar^2 k_F^2/2m)| = 0.815 E_F$, where E_F denotes the Fermi energy. If we take values of $E_F = 11.4$ eV,[37] $\delta = 2.6$ eV,[37] and $|D| = 6.8$ eV,[4] we obtain $|M_1^*(k_F, \hbar^2 k_F^2/2m)| = 9.29$ eV. Using Eq. (5), the inner potential, $|\Sigma_1^*(k_F, \hbar^2 k_F^2/2m)| = 13.5$ eV. Also, using the relationship [see Fig. (4)]

$$E_F + \phi = |M_1^*(k_F, \hbar^2 k_F^2/2m)| + |D|, \tag{7}$$

where ϕ is the work function of the solid, we obtain $\phi = 4.69$ eV. This is to be compared to the experimentally measured value of 4.2 eV obtained from a polycrystalline aluminum surface.

E. Phonons

Phonon excitations at finite temperatures constitute quasielastic processes. This is because

vacuum level

$|D|$ ϕ

$|M_1^*(k_F, \frac{\hbar^2}{2m}k_F^2)|$ E_F $|\Sigma_1^*(k_F, \frac{\hbar^2}{2m}k_F^2)|$

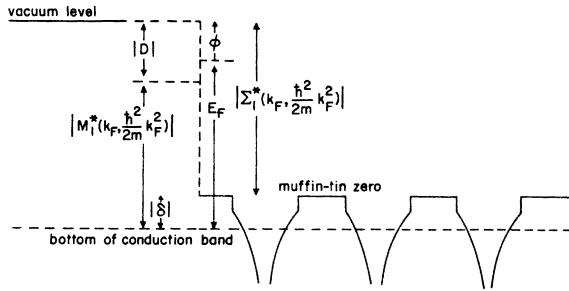muffin-tin zero

$|\delta|$

bottom of conduction band

FIG. 4. Schematic presentation of the inner potential $|\Sigma_1^*(k_F, \hbar^2 k_F^2/2m)|$ at the Fermi level. $|D|$ is the surface dipole, ϕ is the work function, E_F is the Fermi energy, and $|M_1^*(k_F, \hbar^2 k_F^2/2m)|$ is the renormalized exchange-correlation potential. δ is the difference in energy between the muffin-tin zero and the bottom of the conduction band.

phonons have energies much smaller than the initial energy spread of the incident-electron beam. Electrons, after undergoing phonon scatterings, are still collected in the elastically backscattered flux. However, phonons can scatter electrons away from two-dimensional Bragg spots through momentum transfer. This effect is commonly known as thermal diffuse scattering. The process of thermal diffuse scattering removes elastically backscattered electrons from Bragg spots and transfers them into other areas of the fluorescent screen. The decrease in intensity in Bragg spots at finite temperatures is usually expressed in terms of a Debye–Waller factor with a chosen Debye temperature representing characteristic vibrational properties of the solid. In real surfaces, phonon modes at the surface are highly anisotropic,[38-44] with vibrations of ion cores perpendicular to the surface larger than those parallel to the surface. Moreover, vibration amplitudes for phonon modes at surface layers are in general larger than corresponding modes in the bulk.[42,43] In a realistic model for surface vibrations, one should take into account the anisotropic properties of surface phonons as well as their larger vibration amplitudes. Also, ion cores in different surface layers have different mean vibration amplitudes. However, except for the simplest cases,[44,45] such surface-phonon effects are difficult to include. In this calculation, we assume an isotropic model for phonon excitations and express their average effects in terms of a single effective Debye temperature. In principle, one can phenomenalogically include effects of larger surface vibration amplitudes by picking a smaller effective Debye temperature. But, in the absence of a reliable value for the mean surface Debye temperature, we simply use a bulk value of $\Theta_D = 426$ °K in this calculation. Since the isotropic model for surface phonon modes is an extremely

crude one, we retain only the first partial-wave expansion of the Debye–Waller factor.[46] It is obvious that our model for surface vibrations is too crude for any detailed study of temperature effects of LEED spectra.[44,45] However, for the purpose of determining the *energy dependence* of diffraction spectra, our present phonon model is adequate. This is true because the Debye-Waller factor has little effect on position of diffraction peaks. Its main effect is to decrease relative intensities of diffraction peaks at higher energies.

III. LIMITS ON COMPARISON BETWEEN THEORY AND EXPERIMENT

In Sec. II, details of dynamical factors important in a microscopic calculation of LEED spectra are discussed. Such dynamical factors contain uncertainties which would limit the extent to which theory can be meaningfully compared with experiment. In a LEED-spectra comparison between theory and experiment, one is primarily concerned with comparing the following quantities: absolute and relative intensities; and the shape, width, and position of diffraction peaks. Different dynamical factors affect such features in different degrees. The value of the inner potential $\Sigma_1^*(k, \hbar^2 k^2/2m)$ and the one-electron crystal potential determine primarily positions of calculated peaks. The damping strength, $\Sigma_2^*(k, \hbar^2 k^2/2m)$, and the position of the electron-vacuum interface affect the calculated absolute reflectivity. The former quantity also affects widths of diffraction peaks. The shape of the surface barrier affects peak intensities and peak shapes at low energies (e.g., below 50 eV for aluminum). The choice of the surface-phonon model affects peak intensities and shapes at high energies. Finally, the crystal potential affects the shape and intensity of diffraction peaks in the whole energy range.

Let us first examine the accuracy to which peak positions may be determined in present theoretical models. From the energy dependence of $M_1(k, \hbar^2 k^2/2m)$ shown in Fig. 3, we note using Eqs. (4) and (5) that for aluminum, the inner potential $\Sigma_1^*(k, \hbar^2 k^2/2m)$ changes about 6 eV in the energy range from 0 to 200 eV. Also, different crystal potentials place peak positions 3–5 eV differently.[47] For a *conservative* estimate, present dynamical models have an energy uncertainty for peak positions of 5–7 eV in the range 0–200 eV. The magnitude of this uncertainty may appear large, since a purely kinematical model would place Bragg peaks within this same energy range as the experimental peak positions with a properly chosen inner potential. However, a kinematical model totally fails to produce multiple scattering peaks, which from experimental studies of many materials are known to be large.[48-50] It should also be borne in

mind that LEED peaks are generally 8–18 eV wide,[20] hence, even with this large uncertainty in the determination of exact peak positions, it is in most cases not difficult to correlate each calculated peak with the appropriate experimental peak. A more reliable way to identify peaks between theory and experiment is of course to compare spectra for a set of angles of incidence and to examine similarities in the angular evolution of peak profiles with systematic variations in angular orientation.

As for the absolute reflectivity, experimentally measured values for most materials are in the range of a few percent[48,49] of the incident flux. The calculated reflectivity, on the other hand, depends sensitively on the magnitude of electron damping and on where one places the electron-vacuum interface. However, if one chooses damping values either from self-energy calculations,[29,30] or by fitting to experimentally measured half-widths; and if one places the electron-vacuum interface at physically plausible positions like those shown in Fig. 2, one does obtain calculated reflectivities of a few percent for most materials.[20,22,28,48] The agreement in absolute reflectivities for these materials in not precise but one obtains order-of-magnitude agreements. The crucial test for contributions of dynamical factors in terms of absolute reflectivities is in the ability to match theory and experiment for absolute reflectivities of different reflected beams and for a set of incident angles. Another test is to obtain good agreement with predicted and experimental absolute reflectivities for more than one face of the same material for different beams.

There is general agreement between theory and experiment for peak widths and relative intensities to within a factor of 2. The poorest known and perhaps the most uncertain quantity in the calculation of LEED spectra is the exact shape of peaks. The reason for this is that almost all dynamical factors discussed earlier and particularly the crystal potential, affect the shape of diffraction peaks. The models for surface barrier and surface phonons affect shapes of peaks at low- and high-energy regions, respectively. From discussions in Sec. II, present models for these two dynamical quantities are relatively crude. One may eliminate contributions from these quantities by concentrating on high-energy peaks (e.g., above 50 eV for aluminum) at low temperatures. However, peak shapes are also affected by the damping strength, the propagator renormalization factor, and the crystal potential. Thus it is rather difficult to separate unambiguously effects of one dynamical factor from another. For these reasons in terms of present calculations, it seems best not to place too much emphasis on details of peak shapes.

In this section, we have discussed some of the important features in LEED spectra and their relative dependences on different dynamical factors. Reliability tests of a dynamical model lie not in being able to match details of a single spectra for a given angle of incidence in a limited energy range; but in being able to use the same set of dynamical quantities to obtain over-all agreement between theory and experiment for a wide range of energies and incident angles, for many reflected beams as well as for more than one crystal face.

IV. COMPUTATION PROCEDURE OF THE *t*-MATRIX METHOD

In the preceding paper, the formalism of the *t*-matrix method was presented. This method keeps to only finite orders multiple scattering events of the incident electron inside the solid. The physical justification of this approach is that in the presence of strong electron damping, electrons that have undergone a number of scatterings no longer contribute significantly to the intensity of the backscattered elastic current.[28] In the present calculation, we keep multiple scattering events only to third order in the individual ion-core scattering matrix. In other words, we evaluate all the terms given in Eq. (25) of the preceding paper. The complex propagator renormalization factor $F(k_0)$ defined in Eq. (14) of the preceding paper is rewritten in the form

$$F(k_0) = 2k_0 \Big/ \left[2k_0 + \left(\frac{2m}{\hbar^2}\right)\frac{\partial \Sigma(k, E)}{\partial k}\bigg|_{k_0} \right] \quad (8)$$

$$= Z(k_0)\left[2k_0 \Big/ \left(\frac{2m}{\hbar^2}\right)\frac{dE}{dk}\bigg|_{k_0} \right], \quad (9)$$

and evaluated for an electron density corresponding to that of metallic aluminum. A plot of real and imaginary parts of $F(k_0)$ used in this calculation as a function of electron energy measured with respect to the vacuum level is shown in Fig. 5. Partial convergence tests of the *t*-matrix method by comparing scattered intensities containing infinite orders of multiple scattering events in the plane with those including up to third-order scattering events are reported elsewhere.[28,51] The results showed good convergence. It is clear that the *t*-matrix method will begin to fail in the limit of strong ion-core scattering and relatively small inelastic damping. This is because in the presence of strong ion-core scattering and weak damping, the incident electron has a large penetration distance and higher-order scattering events become significant. On the other hand, truncation errors are not serious as long as their magnitudes are small compared with contributions from uncertainties in the many critical dynamical factors dis-
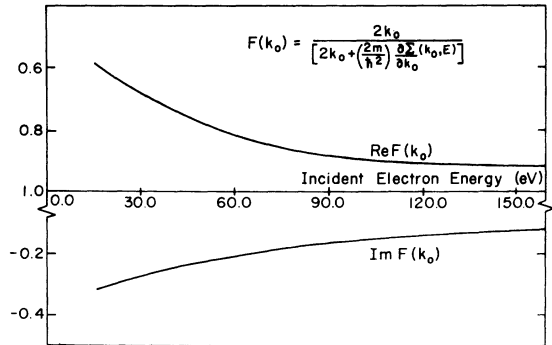
FIG. 5. Energy dependence of the complex propagator renormalization factor $K(k_0)$. The energy scale is measured with respect to the vacuum level.

cussed in Sec. III. Also, a great deal is gained by this finite truncation of multiple scattering events. The t-matrix method for the computation of LEED spectra is very fast and the computation core size is small. This leaves plenty of room for the fuller
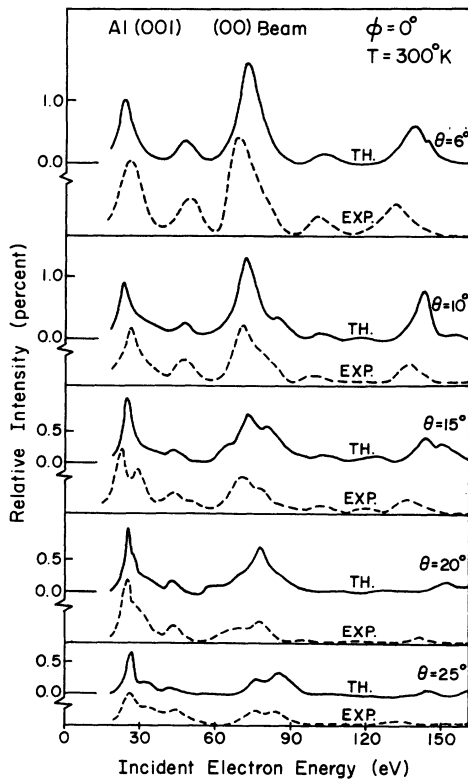
incorporation of other physical quantities important in a microscopic model. One such factor is in the inclusion of the crystal potential in terms of many partial-wave phase shifts. Another example is that inside the crystal, the incident electron scatters into a large number of Bloch wave states. In order to obtain convergence in the representation of the scattered states inside the solid, it is desirable to include a large number of Bloch waves inside the solid. This is one of the most troublesome features in a microscopic approach. In this calculation, because of the small core-size requirement of the t-matrix method, it is possible to include up to 49 Bloch waves in the sums over scattered states. This number of Bloch waves included is significantly larger than any number used before. Nevertheless, these calculations using six partial waves for the scattering potential and 49 Bloch waves[52] take, on the average, only 18 sec per energy point on an IBM 360/65 computer.

V. COMPARISON BETWEEN THEORY AND EXPERIMENT ON Al(001) AND Al(110) FACES

We have calculated LEED spectra in absolute reflectivities for the (001) and (110) faces of aluminum for specular and nonspecular beams for a wide
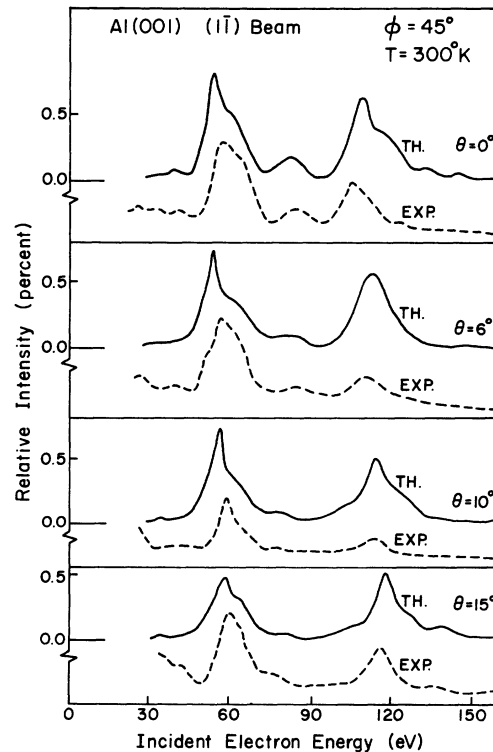

FIG. 6. Comparisons between theory and experiment for Al(001) with reference to the (00) beam for different angles of incidence. Theoretical curves (solid lines) are in absolute reflectivities calculated using six phase shifts at $T = 300$ °K. Experimental curves (broken lines) are taken from room-temperature results of Ref. 53 in arbitrary intensity units.

FIG. 7. Comparisons between theory and experiment for Al(001) with reference to the (1$\bar{1}$) beam, for different angles of incidence. Other conditions are the same as in Fig. 6.

range of angles of incidence in the energy range
0–160 eV. Our theoretical results are compared
with experimental measurements made by Jona.[50]
Calculations for the spectra were made in 5-eV
intervals. The comparisons are shown in Figs.
6–12.[53]

A. Al(001) Face

Comparisons for the (00) beam for five angles of
incidence are shown in Fig. 6. The calculated
spectra are of the order of 1% in absolute reflectiv-
ities. The experimental measurements were not
made on the absolute scale. There is good agree-
ment, however, in peak widths, relative intensities,
and angular evolution of peak profiles. The biggest
discrepancy between theory and experiment occurs
for the beam at $\theta = 15°$, where the experiment shows
a split peak at 26 eV which is absent in the theo-
retical curve. Also, the experimental peak at 137
eV is not split, although the calculation indicates a
split structure there. It is interesting to note that
a more recent measurement by Quinto and Robert-
son[54] for Al(001) at the same azimuth and angle of
incidence shows the peak at 137 eV to be markedly
split. More detailed theoretical and experimental
investigations are needed before any definite conclu-
sions can be drawn on this point.
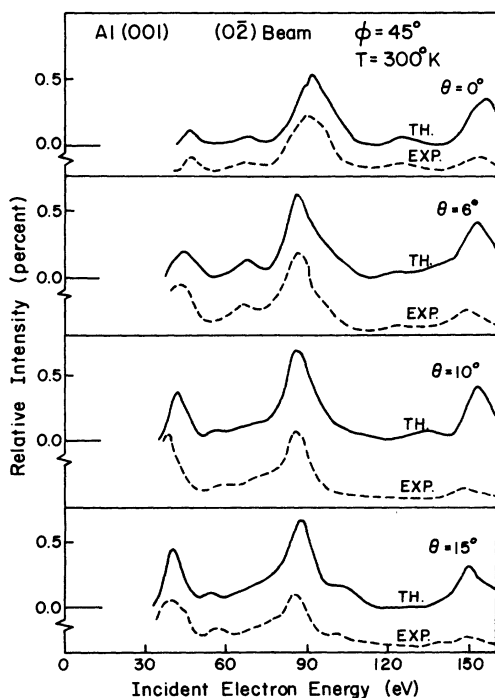
The agreement between theory and experiment

FIG. 8. Comparisons between theory and experiment
for Al(001) with reference to the (0$\bar{2}$) beam, for different
angles of incidence. Other conditions are the same as in
Fig. 6.

is also good on this face for the (1$\bar{1}$) and (0$\bar{2}$) beams
for different angles of incidence (Figs. 7 and 8).
Looking at high-energy peaks, e. g. , at around 130
eV for the (00) beam, 105 eV for the (1$\bar{1}$) beam,
and 152 eV for the (0$\bar{2}$) beam, the experimental
peaks are consistently lower in intensity than the
corresponding theoretical peaks for all angles of
incidence. This may not be surprising if one re-
calls that in our dynamical model, we have used a
high (bulk) Debye temperature of $\Theta_D = 426$ °K. This
value of the effective Debye temperature is definite-
ly a lower limit of surface-phonon vibration ampli-
tudes. A smaller effective Debye temperature
corresponding to larger and more realistic phonon
vibration amplitudes will improve the agreement in
intensities in the high-energy region.

LEED intensity spectra for Al(001) face have
been also calculated by Jepsen et al.[26] and Lara-
more et al.[27] They obtained similar degrees of
general good qualitative agreement with experi-
ment. In calculations done by Jepsen et al. ,[26] they
used a self-consistent band-structure potential by
Snow,[55] which is a stronger bulk potential than the
one we used here. On account of this, Jepsen
et al.[26] obtained somewhat more prominent secon-
dary features in the intensity spectra. However,
it is difficult at this stage to draw any more definite
conclusions on the superiority of different bulk po-
tentials used by Jepsen et al. ,[26] Laramore et al. ,[27]
and others in their application to LEED calcula-
tions. Perhaps the most significant difference in
terms of input parameters between these other cal-
culations and those of this study is our inclusion
of an energy-dependent complex propagator re-
normalization factor $F(k_0)$. We find by using $F(k_0)$
evaluated from electron-gas calculation for alumi-
num, the qualitative features of the LEED spectra
are generally improved.[56]

B. Al(110) Face

The agreement between theory and experiment is
not as good for this face as for the (001) face. It
is found necessary to shift the energy scale of the
experimental curves or to change the value of the
inner potential in the theoretical model to obtain
good correspondence in peak positions. For the
(00) beam, shown in Fig. 9, we have shifted the
experimental curves to lower values by 7 eV with
respect to the theoretical curves.[57] Otherwise, the
same (energy-dependent) inner-potential values   ·
used for the (001) face are used here for the (110)
face in the theoretical model. In other words, the
relatively small change in work function on differ-
ent crystal faces is neglected here. With the 7-eV
downshift, while the peaks at 68. 6 eV are in agree-
ment with experiment, the lower-energy peaks at
26 eV are off in position. In a recent work by Jep-
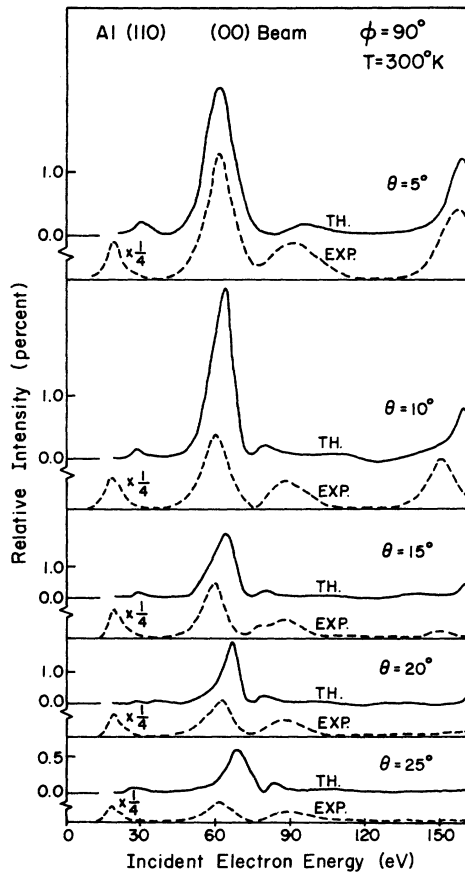sen et al. ,[58] they also concluded that a shift in en-

FIG. 9. Comparisons between theory and experiment for Al(110) with reference to the (00) beam, for different angles of incidence. The experimental curves are shifted down in energy by 7 eV. Other conditions are the same as in Fig. 6.

ergy produces better agreement in peak positions. They used an upshift of their theoretical curves of 3.7 eV. This is because in their work, they chose to line up the peaks at 26 eV. An interesting analysis suggesting steps in the crystal surface was recently proposed to explain this effect.[59] It is also interesting to note that the experimental peak at 68.6 eV stays almost constant in energy as the angle of incidence increases from $\theta = 5°$ to $\theta = 25°$. The corresponding theoretical peak, on the other hand, increases in energy with increasing incident angle. This is because the theoretical "Bragg" energy increases with increasing angle.

Comparisons for the ($\bar{1}\bar{1}$) and (10) beams for Al(110) are shown in Figs. 10 and 11. The experimental curves in the ($\bar{1}\bar{1}$) beam are shifted down in energy by a constant 3 eV[60] while those in the (10) beam are shifted down by 7 eV. For the ($\bar{1}\bar{1}$) beam, the experimental curves show a much larger peak at low energies ($E \approx 35$ eV). Similarly, for the (10) beam, the agreement for peaks at low energies
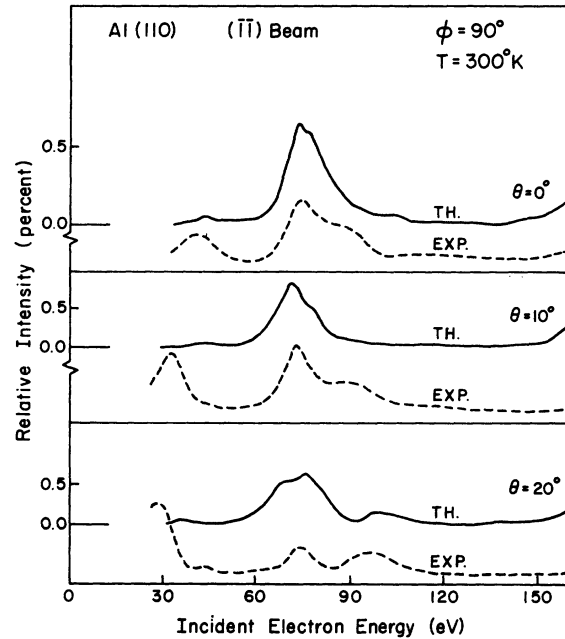

FIG. 10. Comparisons between theory and experiment for Al(110) with reference to the ($\bar{1}\bar{1}$) beam, for different angles of incidence. The experimental curves are shifted down in energy by 3 eV. Other conditions are the same as in Fig. 6.

($E \approx 50$ eV) is poor. The agreement is generally good for higher energies.
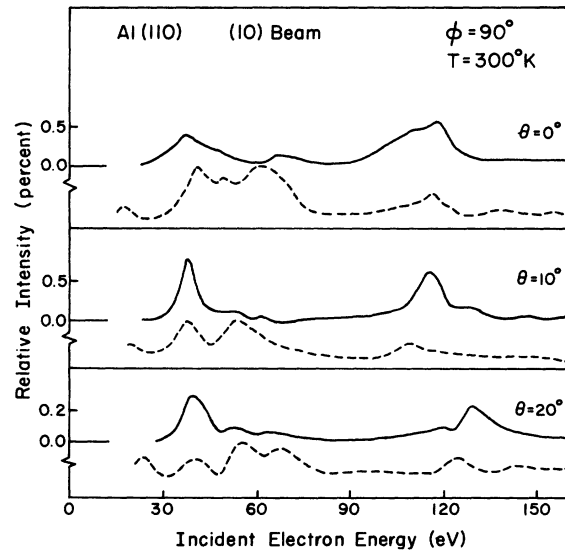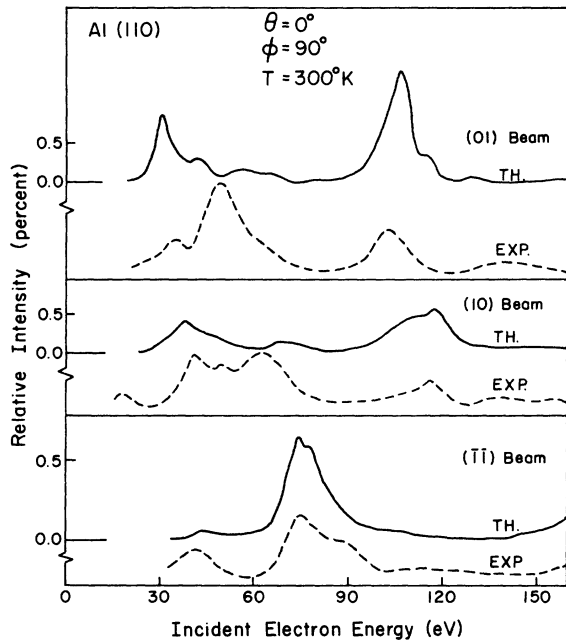
Finally, in Fig. 12, we show the (01), (10), and

FIG. 11. Comparisons between theory and experiment for Al(110) with reference to the (10) beam, for different angles of incidence. The experimental curves are shifted down in energy by 7 eV. Other conditions are the same as in Fig. 6.

FIG. 12. Comparisons between theory and experiment for Al(110) with reference to the (01), (10), (1̄1̄) beams at normal incidence. The experimental (01) curve is shifted down in energy by 7 eV. Curves for (10) and (1̄1̄) beams are the same as the corresponding ones shown in Figs. 11 and 10. Other conditions are the same as in Fig. 6.

(1̄1̄) beams for Al(110) at normal incidence. The experimental (01) curve is shifted down in energy by 7 eV. Once again, the agreement at low ener-

gies ($E \approx 55$ eV) for this beam is rather poor.

VI. SUMMARY

We have used the *t*-matrix perturbation method to calculate LEED spectra for the (001) and (110) faces of aluminum. Agreement between theory and experiment for different beams and a wide range of incident angles appears to be good, especially on the (001) face. On the (110) face, there are some discrepancies in peak positions and in peak profiles at low energies. Interpretations of such discrepancies in terms of surface expansion[27,58] and of random steps on the surface[59] have been recently proposed. It is also possible that other effects, such as impurities in the surface region and effects of surface plasmons may be partly responsible for such discrepancies.

The *t*-matrix method as presented here seems to work well for the dynamical model chosen for aluminum. Convergence tests of this method with an equivalent exact method to establish limits of the perturbation approach are in progress. These results will be reported separately. It is significant that the success of a perturbation approach in LEED-spectra calculations opens the way to new practical applications of low-energy-electron diffraction in the study of surface atomic structure. It seems more feasible for LEED-spectra calculations to be carried out on a routine and practical basis for clean metals using the *t*-matrix approach. Extension of the perturbation method to clean surfaces of transition metals and to chemical overlayers on metals are also under current investigation and will be reported separately.

[1]P. W. Palmberg and T. N. Rhodin, J. Appl. Phys. **39**, 2425 (1967).

[2]C. B. Duke and C. W. Tucker, Jr., Surf. Sci. **15**, 231 (1969); C. B. Duke, J. R. Anderson, and C. W. Tucker, Jr., Surf. Sci. **19**, 117 (1970).

[3]J. A. Strozier, Jr. and R. O. Jones, Phys. Rev. Lett. **25**, 516 (1970).

[4]N. D. Lang and W. Kohn, Phys. Rev. B **1**, 4555 (1970); Phys. Rev. B **3**, 1215 (1971).

[5]J. A. Appelbaum and D. R. Hamann (unpublished).

[6]See, for example, Refs. 1–8 and 10–13 of preceding paper.

[7]J. R. Schrieffer, J. Vac. Sci. Technol. **9**, 561 (1971); J. R. Schrieffer and R. Gomer, Surf. Sci. **25**, 315 (1971).

[8]R. H. Paulson and J. R. Schrieffer (unpublished).

[9]T. L. Einstein and J. R. Schrieffer (unpublished).

[10]J. W. Gadzuk, Surf. Sci. **6**, 133 (1967); J. W. Gadzuk, J. K. Hartman, and T. N. Rhodin, Phys. Rev. B **4**, 241 (1971).

[11]D. M. Newns, Phys. Rev. **178**, 1123 (1969); Phys. Rev. B **1**, 3304 (1970).

[12]A. J. Bennett, B. McCarroll, and R. P. Messmer, Phys. Rev.

B **3**, 1397 (1971); Surf. Sci. **24**, 191 (1971).

[13]E. W. Plummer and R. D. Young, Phys. Rev. B **1**, 2088 (1970); E. W. Plummer and A. E. Bell, J. Vac. Sci. Technol. **9**, 583 (1971).

[14]D. E. Eastman and J. K. Becker, Phys. Rev. Lett. **27**, 1520 (1971); D. E. Eastman and W. D. Grobman, Phys. Rev. Lett. **28**, 1327 (1972); Phys. Rev. Lett. **28**, 1378 (1972).

[15]L. F. Wagner and W. E. Spicer, Phys. Rev. Lett. **28**, 1381 (1972).

[16]H. D. Hagstrum and G. E. Becker, Phys. Rev. Lett. **22**, 1054 (1969); J. Chem. Phys. **54**, 1015 (1971).

[17]G. E. Becker and H. D. Hagstrum, Surf. Sci. **30**, 505 (1972).

[18]C. B. Duke and G. E. Laramore, Phys. Rev. B **3**, 3183 (1971); Phys. Rev. B 3, 3198 (1971).

[19]A. Bagchi and C. B. Duke (unpublished).

[20]S. Y. Tong and T. N. Rhodin, Phys. Rev. Lett. **26**, 711 (1971).

[21]J. B. Pendry (private communication).

[22]J. B. Pendry, J. Phys. C **4**, 2501 (1971); J. Phys. C 4, 2514 (1971).

[23]G. Capart, Surf. Sci. **26**, 429 (1971).

[24]See, for example, Eq. (2) of preceding paper.

[25]L. A. Maccoll, Phys. Rev. **56**, 699 (1939).

[26]D. W. Jepsen, P. M. Marcus, and F. Jona, Phys. Rev. B **5**, 3933 (1972).

[27]G. E. Laramore and C. B. Duke, Phys. Rev. B **5**, 267 (1972).

[28]R. H. Tait, S. Y. Tong, and T. N. Rhodin, Phys. Rev. Lett. **28**, 553 (1972).

[29]J. J. Quinn, Phys. Rev. **126**, 1453 (1962).

[30]B. I. Lundqvist, Phys. Status Solidi **32**, 273 (1969).

[31]S. Y. Tong, T. N. Rhodin, and R. H. Tait, preceding paper, Phys. Rev. B 8, 421 (1973); on formulation of the t-matrix approach.

[32]S. Y. Tong and T. N. Rhodin, in Proceedings of the Fifth LEED Seminar, Washington, D. C., 1971 (unpublished).

[33]A. W. Overhauser, Phys. Rev. B **3**, 1888 (1971).

[34]E. C. Snow, Phys. Rev. **158**, 683 (1967).

[35]W. A. Harrison, Phys. Rev. **118**, 1182 (1960).

[36]V. Heine, Proc. R. Soc. A **240**, 361 (1957).

[37]B. Segall, Phys. Rev. **124**, 1797 (1961).

[38]A. A. Maradudin, Solid State Phys. **18**, 1 (1966).

[39]B. C. Clark, R. Herman, and R. F. Wallis, Phys. Rev. **139**, A860 (1965).

[40]S. Y. Tong and A. A. Maradudin, Phys. Rev. **181**, 1318 (1969).

[41]T. S. Chen, G. P. Alldredge, and F. W. de Wette, Phys. Rev. Lett. **26**, 1543 (1971).

[42]R. E. Allen and F. W. de Wette, Phys. Rev. **179**, 873 (1969).

[43]R. E. Allen, F. W. de Wette, and A. Rahman, Phys. Rev. **179**, 887 (1969).

[44]A. Ignatiev, T. N. Rhodin, S. Y. Tong, B. I. Lundqvist, and J. B. Pendry, Solid State Commun. **9**, 1851 (1971).

[45]A. Ignatiev, T. N. Rhodin, and S. Y. Tong, Bull. Am. Phys. Soc. **17**, 634 (1972); A. Ignatiev, T. N. Rhodin, and S. Y. Tong, Phys. Rev. (to be published).

[46]See, for example, Eq. (6) of preceding paper.

[47]See, for example, Tables I–III, Ref. 27.

[48]J. E. Demuth, S. Y. Tong, and T. N. Rhodin, J. Vac. Sci. Technol. **9**, 639 (1972).

[49]S. Andersson, Surf. Sci. **18**, 325 (1969).

[50]F. Jona, IBM J. Res. Dev. **14**, 444 (1970).

[51]S. Y. Tong, T. N. Rhodin, and R. H. Tait, Proceedings of the Sixth LEED Seminar, Washington, D. C., 1972. See also Surf. Sci. 34, 457 (1973).

[52]Our previous specification of 29 beams made in Ref. 28 should be changed to 49 beams.

[53]In Figs. 6–12, some of the experimental curves are slightly different from those shown in Ref. 50, especially at low energies. This is because we have used in this work updated experimental outputs sent to us by F. Jona.

[54]D. T. Quinto and W. D. Robertson, Surf. Sci. (to be published).

[55]E. C. Snow, Phys. Rev. **158**, 683 (1967).

[56]S. Y. Tong, G. E. Laramore, and T. N. Rhodin (unpublished).

[57]In Ref. 28, we reported a shift of the experimental curves down by 12 eV. This is because there we read off energies from the experimental curves in Ref. 50. Using the more accurate experimental outputs in this work (see also Ref. 53), we find a smaller shift of 7 eV is best.

[58]D. W. Jepsen, P. M. Marcus, and F. Jona (unpublished).

[59]G. E. Laramore, J. E. Houston, and R. L. Park (unpublished).

[60]The intensity scales for absolute reflectivities for the (00) and (11) beams of Al(110) in Ref. 28 should be multiplied by a factor of 2.

Surfaces of Transition Metals

Peter Fulde

Institut Max von Laue-Paul Langevin, 8046 Garching, Germany

A. Luther*

Harvard University, Cambridge, Massachusetts 02138

R. E. Watson

Brookhaven National Laboratory,[†] Upton, New York 11973

We study the properties of transition-metal surfaces, with particular emphasis on Ni. Using the renormalized-atom approach, it is argued that the d-state excitations are narrowed at the surface and the d-hole count is reduced. The magnetic coupling of the surface layer to bulk is investigated in detail. Spin-dependent surface resonances of the Friedel type can exist and in the magnetic metals, can cause antiferromagnetic coupling of the surface moment to bulk. Model calculations are presented in an attempt to describe Ni.

I. INTRODUCTION

Relatively little progress has been made towards an understanding of the electronic states at the surface of a d transition metal. These states are important for a determination of many surface properties,[1] chemisorption, and catalysis. In addition, recent electron-emission and tunneling experi-ments[2] designed to probe bulk-metal properties have yielded results which suggest some partici-pation of surface states. It is the purpose of this paper to discuss the electronic and magnetic prop-erties of these states within the framework of ex-isting theories of transition metals, with particular emphasis on Ni.

In Sec. II, the electronic properties of the para-